Single-Layer Wideband Circularly Polarized High-Efficiency Reflectarray for Satellite Communications

Long Zhang, Steven Gao, *Senior Member, IEEE*, Qi Luo, *Member, IEEE*, Wenting Li, Yejun He, *Senior Member, IEEE,* and Qingxia Li, *Member, IEEE*

***Abstract*— This paper presents a single-layer circularly polarized reflectarray which achieves large bandwidth (BW) in terms of axial ratio (AR), gain, aperture efficiency (AE) and radiation pattern. By using a novel wideband S-shaped phasing element, an offset-fed reflectarray with 20° offset beam is designed based on the element angular rotation method. Theoretical analysis is given to analyze the effect of angular rotated elements on the performance of the reflectarray, which indicates that the AR BW of the reflectarray can exceed the AR BW of the feed horn. Furthermore, the influence of the differential spatial phase delay is analyzed quantitatively, and the performance of S-element-based reflectarrays with different aperture sizes are investigated and discussed. To verify these concepts, a 180 mm × 180 mm prototype with 15 × 15 elements is fabricated and measured. The measured results confirm that the proposed reflectarray achieves a 68.5% 3-dB AR BW (7 to 14.3 GHz) and a 47.8% 3-dB gain BW (8.6 to 14 GHz). Moreover, the AE is larger than 50% in a 33% BW and larger than 30% in a 64% BW.**

***Index Terms*— Circular polarization, element rotation method, reflectarray, satellite communications, wideband array.**

I. Introduction

PRINTED reflectarrays combine the advantages of parabolic antennas and planar phased arrays, which receive increasing interest in designing high-gain antennas. Generally, reflectarrays consist of radiating elements with preadjusted phases and an illuminating feed antenna to form a planar phase front in the far field [1]. Although they have many advantages, such as the significantly simplified feeding system, versatile beams, flat structure, and low manufacturing cost, one major drawback of reflectarrays is their narrow BW.

The narrow BW of reflectarrays is mainly caused by two factors: the inherent narrow BW of microstrip elements and the differential spatial phase delay caused by different path lengths from the feed to each element [2]. To improve the BW of reflectarrays, several approaches were adopted, such as using stacked patches [3], subwavelength element [4], dual-frequency phase synthesis [5], and true time delay technique [6].

Designing circularly polarized (CP) reflectarray is necessary for some applications since the CP arrays possess the advantages of mitigation of multipath fading, immunity of "Faraday rotation" and the reduction of polarization mismatching [7]. Two different ways have been introduced to design a CP reflectarray. The first one is using a linearly polarized (LP) feed to illuminate an aperture which is able to transform the incident LP wave to CP reflected wave and form a cophasal beam in the far field [8], [9]. Another method to design a CP reflectarray is utilizing a CP feed as a primary source and the reflected wave can superpose in-phase in the far field. Various designs based on this approach were proposed, including using angular rotated elements [10], [11], variable sized elements [12], and elements with variable-length phase delay lines [13].

Considering that it is more difficult to design elements with wideband CP reflection performance and wideband CP feeds, the BW enhancement of CP reflectarrays is thus more challenging than LP reflectarrays. To meet frequency coverage requirement, designing dual-frequency CP reflectarrays is attractive to some applications [14], [15]. However, for applications such as high-data-rate satellite communications, it is highly desirable to have CP reflectarrays with broad BW [16]. Different approaches were utilized to improve the BW of CP reflectarrays [9], [17]–[20]. Through using rectangular-patch phasing element with subwavelength grid spacing, a 17% 1-dB gain BW and a 11% 3-dB axial ratio (AR) BW were obtained [17]. The BW of CP reflectarrays was further improved by using a dual-layer T-shaped phasing element, with a 1-dB gain BW of 20% and 3-dB AR BW of 28% [18]. Since the elements used in [17] and [18] are resonant type, the CP reflectarray using these resonant phasing elements demonstrates a typically smaller than 30% BW. Multiresonance phasing elements such as the Jerusalem cross

Manuscript received December 14, 2016; revised May 22, 2017; accepted June 17, 2017. Date of publication July 3, 2017; date of current version September 1, 2017. This work was supported in part by the U.K. Engineering and Physical Sciences Research Council under Grant EP/N032497/1, in part by the National Natural Science Foundation of China under Grant 61372077, in part by the Science and Technology Innovation Commission of Shenzhen under Grant ZDSYS 201507031550105, and in part by Guangdong Provincial Science and Technology Programs under Grant 2013B090200011 and Grant 2016B090918080. *(Corresponding author: Wenting Li.)*

L. Zhang and Y. He are with the Shenzhen Key Laboratory of Antennas and Propagation and the Guangdong Engineering Research Center of Base Station Antennas and Propagation, College of Information Engineering, Shenzhen University, Shenzhen 518060, China (e-mail: longzhang717@163.com; heyejun@126.com).

S. Gao, Q. Luo, and W. Li are with the School of Engineering and Digital Arts, University of Kent, Canterbury CT2 7NT, U.K. (e-mail: s.gao@kent.ac.uk).

Q. Li is with the School of Electronic Information and Communications, Huazhong University of Science and Technology, Wuhan 430074, China.

Color versions of one or more of the figures in this paper are available online at http://ieeexplore.ieee.org.

Digital Object Identifier 10.1109/TAP.2017.2722824

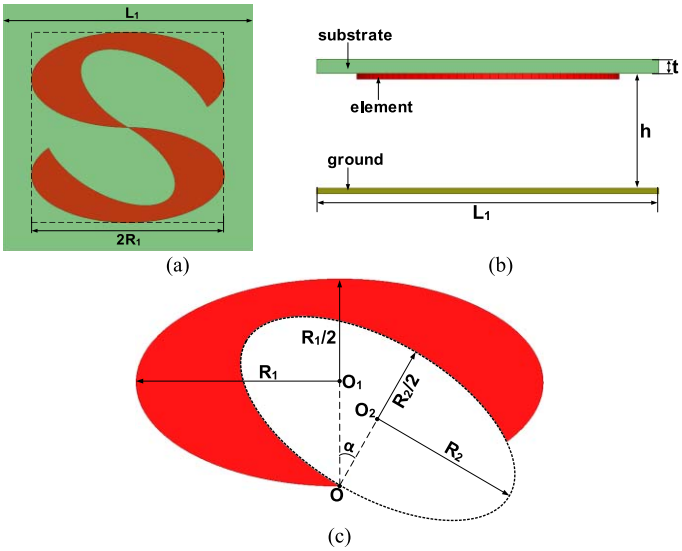

Fig. 1. Geometry of the proposed element. (a) Top view. (b) Side view. (c) Single arm.

and open loop combined subwavelength element [9] and the dual-ring element-based [19] CP reflectarrays achieved more than 30% 3-dB AR BW. Another way to realize wide BW of CP reflectarrays is using spatial time-delay units (TDUs) [20]. Although the CP reflectarray using TDUs achieved 40% 3-dB gain BW and 3-dB AR BW, the aperture efficiency (AE) was just around 40% and the multilayer structure increased the fabrication complexity.

In this paper, a novel S-shaped phasing element which achieves smaller than -15 dB cross polarization (cross-pol) reflection in a 2:1 BW is proposed. Based on this novel broadband element, a single-layer CP reflectarray using angular rotated elements is designed, fabricated, and measured. The measured results indicate that the proposed single-layer reflectarray achieves a 68.5% 3-dB AR BW and a 47.8% 3-dB gain BW. Moreover, the AE is larger than 50% in a 33% BW and larger than 30% in a 64% BW. To the best knowledge of the authors, it is the widest BW single-layer CP reflectarray developed up to now in terms of 3-dB AR and larger than 50% AE BW.

This paper is organized as follows. Section II introduces the design of the novel S-shaped element for reflectarrays. Section III presents the design and analysis of the proposed CP reflectarray. Section IV presents the simulation and measurement results and comparisons with other reported wideband CP reflectarrays. The conclusion is in Section V.

II. S-Shaped Element for Reflectarrays

Various elements have been designed and deployed in CP reflectarrays, such as the patches, stacked patches, crossed dipoles and their derivatives, split rings, and the combination of several types of these elements. All these reported elements demonstrate BWs less than 50%. In this section, a novel S-shaped element for reflectarray application is presented and analyzed, which can achieve a BW over 66%.

A. Element Geometry

The geometry of the proposed S-shaped element is shown in Fig. 1. As shown in Fig. 1(a) and (b), the proposed element is printed on the bottom layer of a Rogers RO4003C substrate with relative dielectric constant of 3.55, dissipation factor of 0.0027, and a thickness of t. A ground plane is placed below the substrate with a height of h which affects the element reflection performance substantially. The element is printed below the substrate in order to achieve better element reflection performance with an integral value of h, which facilitates the prototype fabrication. The size of the ground plane and the unit cell are $L_1 \times L_1$. The S-shaped element is composed of two single arms with the same size shown in Fig. 1(c). It can be seen from Fig. 1(c) that each arm is obtained by subtracting a smaller sized ellipse with a rotating angle α from a larger sized ellipse. To form a square-sized S-shaped element, the major radius of the bigger ellipse R_1 is two times as large as the minor radius.

TABLE I
Element Dimensions

L_1	R_1	R_2	α	h	t
12mm	4.6mm	3.45mm	30°	4mm	0.508mm

The proposed element is a follow-on work of the antenna presented in [21], where an inverted S-shaped antenna with wideband CP radiation was presented. However, there are significant differences between the proposed element and the antenna in [21]. The element proposed in this paper is used for reflectarray application and its reflection performance under periodical boundary environment is of major interest. The proposed phasing element has a more compact size ($0.32\lambda \times 0.32\lambda$) than the antenna presented in [21] ($0.99\lambda \times 0.42\lambda$). The size reduction is realized by choosing bigger rotating angle α and bigger R_1/R_2 ratio, which gives longer traveling-wave current path and the utilization of subwavelength technique. Although the size of the presented element is greatly reduced, the CP BW is largely improved by 58.8% (from 42% in [21] to 66.7%). Furthermore, the proposed element can be placed in a square lattice while the antenna in [21] is only able to be placed in a rectangular lattice. The square-sized element is more advantageous to planar arrays because the rectangular-sized antenna has different electrical lengths along x-axis and y-axis directions, which results in uneven characteristics such as different beamwidths and AR beamwidths in the two orthogonal directions. On the contrary, the proposed element can provide relatively symmetry performance along x-axis and y-axis directions, which brings more equal mutual coupling between each elements in the two directions and thus facilitates the design and improves the performance of the reflectarray.

The detailed geometry dimensions of the proposed element are shown in Table I.

B. Element Performance

As the electrical length of the proposed element is mainly determined by geometry parameters R_1, R_2, and rotating angle α, the impact of these parameters to the element's performance needs to be investigated. For a brief investigation, the ratio $R_2/R_1 = 0.75$ and the rotating angle α is kept unchanged while only R_1 is varied.

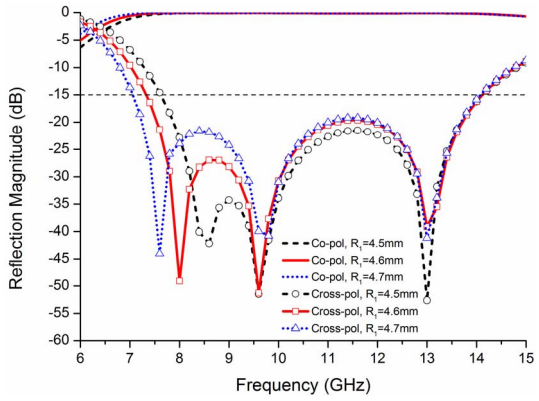

Fig. 2. Magnitude of the reflected field with different R_1.

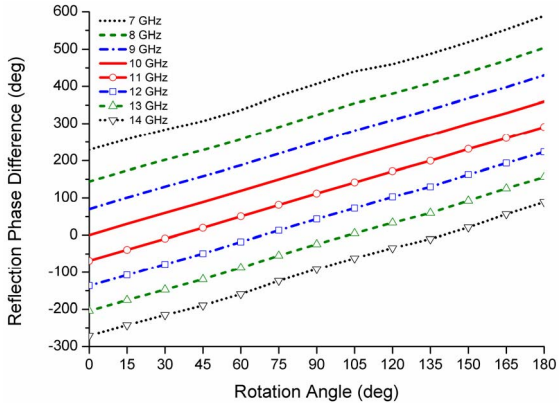

Fig. 3. Phase difference of the reflected co-pol field with different element rotation angles.

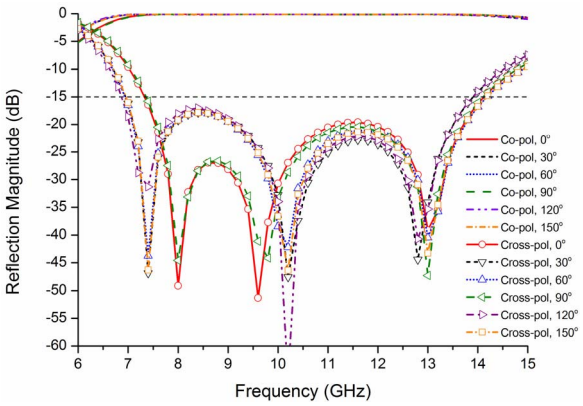

Fig. 4. Magnitude of the reflected field with different rotation angles.

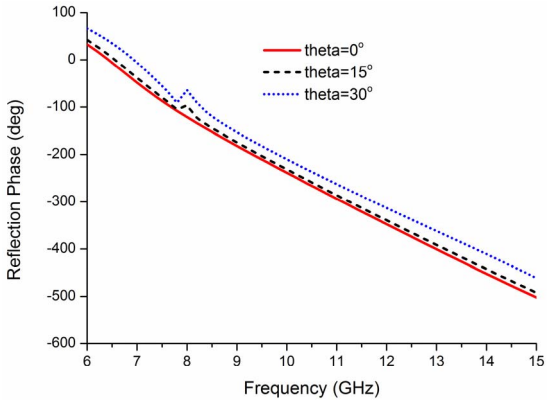

Fig. 5. Reflection phase of the co-pol field with different oblique incidence angles.

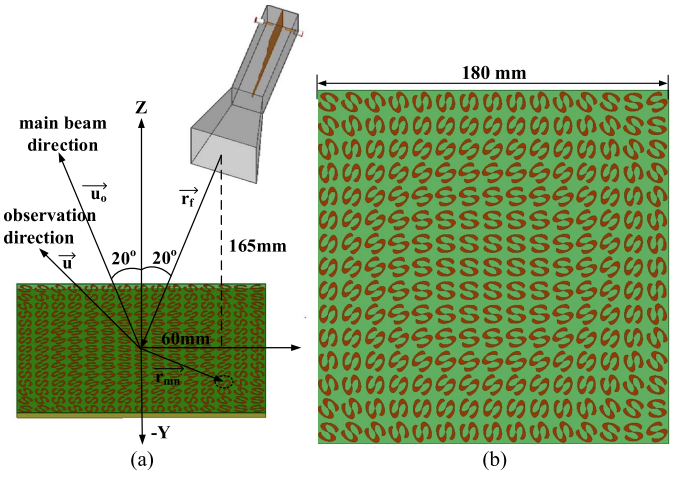

Fig. 6. Configuration of the proposed reflectarray. (a) Side view and (b) top view of reflecting aperture.

The evaluation of the element performance is conducted by using a periodic boundary and a Floquet port excitation in high frequency structure simulator (HFSS) under normal incident plane waves. The incident field is set to be right-hand CP (RHCP). Fig. 2 shows the magnitudes of reflected RHCP field (co-pol component) and left-hand CP (LHCP) field (cross-pol component) with different R_1. As shown in Fig. 2, the available BW ($|\Gamma_{\text{cross-pol}}| \leq -15$ dB) of the element increases with larger R_1. As the ratio R_2/R_1 is kept unchanged, this phenomenon can be explained that increasing R_1 brings longer electrical length and pushes the lowest-frequency resonance to lower frequency.

As shown in Fig. 2, the element can provide a BW of 2:1 (7 to 14 GHz) within which the reflected LHCP component is smaller than -15 dB ($|\Gamma_{\text{cross-pol}}| \leq -15$ dB) when R_1 is 4.7 mm. Notice that $|\Gamma_{\text{cross-pol}}|^2 + |\Gamma_{\text{co-pol}}|^2 \cong 1$ (the approximation rises from dielectric and conductor losses), thus $|\Gamma_{\text{cross-pol}}| \leq -15$ dB makes $|\Gamma_{\text{co-pol}}| \geq -0.2$ dB. To acquire lower cross-pol component reflection and adequate BW simultaneously, R_1 is chosen to be 4.6 mm, which achieves an available BW from 7.3 to 14.1 GHz and $|\Gamma_{\text{cross-pol}}| \leq -20$ dB, $|\Gamma_{\text{co-pol}}| \geq -0.1$ dB from 7.5 to 13.7 GHz.

The element angular rotation method is used to provide the desired phases for each element. It is indicated that the angular rotation angle ψ of a CP element results in a 2ψ phase variation of the reflected co-pol field [10], [22]. Fig. 3 shows the phase difference of the reflected co-pol field under different element rotation angles. As shown in Fig. 3, the element achieves a rather linear phase response to the element rotation angle ψ in a 2:1 frequency range. The phase error (actual phase difference compared with 2ψ) is smaller than 10° within the BW.

The reflection magnitudes of the co-pol and cross-pol components with different rotation angles ψ are shown in Fig. 4. As shown in Fig. 4, the proposed element maintains low cross-pol and good co-pol reflection in a nearly 2:1 frequency range under all rotation angles.

To give an understanding of the element reflection performance under oblique incidence, Fig. 5 shows the reflection phase of the co-pol field under different oblique incidence angle thetas. As shown in Fig. 5, the phase discrepancy of about 7° and 28° are observed for theta = 15° and theta = 30° incidence at the design frequency 9 GHz, respectively. It is noticed that a ripple occurs at the frequency around 8 GHz, which is assumed to be the main reason of the variation of simulated AR and gain at 8 GHz shown in Figs. 8 and 9, respectively. Besides, it is observed from simulation that the phase error is smaller than 10° at 9 GHz under 30° oblique incidence when the element is rotated, which yields not so big differences compared with the case under normal incidence. Considering that only the edge elements are illuminated at large incidence angle, thus the proposed reflectarray is designed based on the reflection phase under normal incident plane waves.

III. Reflectarray Design and Analysis

In this section, the array configuration and the element phase distribution over the aperture are given. Then, the performance of the proposed reflectarray is analyzed theoretically and the conclusions are verified by using different feed horns. Finally, the effects of the differential spatial phase delay and the aperture size on the BW of the proposed reflectarray are analyzed.

A. Array Configuration

The configuration of the proposed reflectarray is shown in Fig. 6. As shown in Fig. 6, the reflectarray consists of 225 (15×15) S-shaped elements, each with different rotation angles to provide required phase delay. The reflectarray is designed to be fed by a wideband dual-CP horn with an offset of 20° to the Z-axis, which is aimed to minimize the blockage of the feed. It is indicated in [23] that an offset feed causes main beam scan with frequency due to a change in phase taper across the reflectarray with a change in frequency. This beam squint phenomenon can be minimized if the angle of the main beam is chosen to be close to the natural specular reflection angle. To eliminate the beam squint, the main beam direction is designed to $\theta = -20°$. The focus-to-diameter ratio (f/D) of 0.97 is chosen to provide an illumination with around -10-dB edge tapering, which helps achieve good BW performance.

The required phase distribution of each S-shaped element is shown in Fig. 7. As the element rotation angle ψ results in a 2ψ phase variation of the reflected co-pol field, the phase distribution in Fig. 7 can directly map into Fig. 6(b).

B. Analysis of Array Performance Using Angular Rotated Elements

It is implicit that the cross-pol of a reflectarray using element angular rotation method is degraded in the main beam region and thus the AR performance can be enhanced [10]. However, this phenomenon is not discussed in detail. Besides, the reflectarray proposed in [10] is a narrowband array, it is important to investigate whether this phenomenon still exists in a wideband reflectarray.

When a 2-D planar array with 15×15 elements is nonuniformly illuminated by a horn at r_f, as shown in Fig. 6(a), the reradiated field from the array in an arbitrary direction $\vec{u}$ can

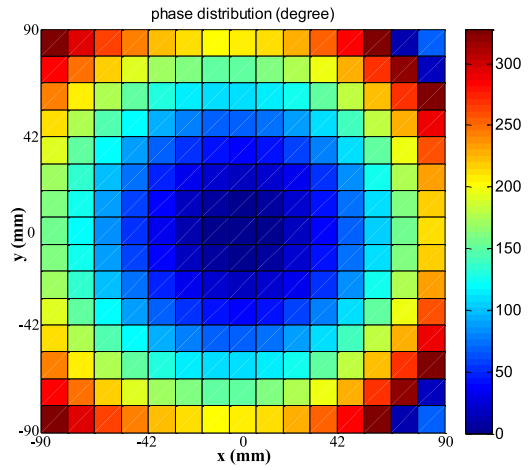

Fig. 7. Required phase distribution for each element.

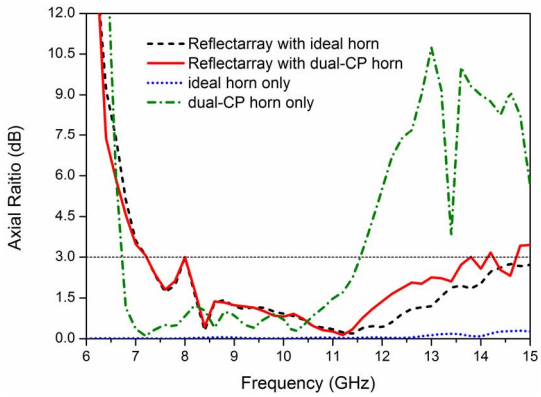

Fig. 8. Simulated AR of the proposed reflectarray with different feed horns.

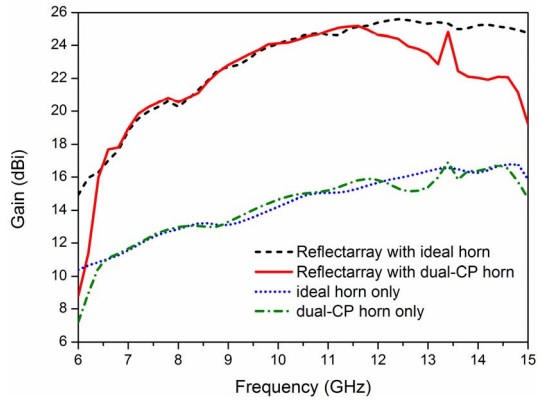

Fig. 9. Simulated gain of the proposed reflectarray with different feed horns.

be represented by

$$E(\vec{u}) = \sum_{m=1}^{15}\sum_{n=1}^{15} F(\overrightarrow{r_{mn}}\cdot\overrightarrow{r_f})A(\overrightarrow{r_{mn}}\cdot\overrightarrow{u_0})A(\vec{u}\cdot\overrightarrow{u_0}) \cdot e^{-jk_0(|\overrightarrow{r_{mn}}-\overrightarrow{r_f}|+\overrightarrow{r_{mn}}\cdot\vec{u})}\cdot e^{j\phi_{mn}} \quad (1)$$

where F is the pattern function of the feed horn, A is the pattern function of the S-shaped element, $\overrightarrow{r_{mn}}$ is the position vector of the mnth element, $\overrightarrow{u_0}$ is the desired main beam direction, k_0 is the free-space wavenumber, and ϕ_{mn} is the required phase delay of the mnth element [10], [24].

Considering an incident wave radiated by the feed horn propagating in the $-Z$ direction, as shown in Fig. 6(a)

$$\vec{E}^{\text{inc}} = F_{\text{RH}}\big(\overrightarrow{E_x} - j\overrightarrow{E_y}\big)e^{jk_0z}e^{j\omega t} + F_{\text{LH}}\big(\overrightarrow{E_x} + j\overrightarrow{E_y}\big)e^{jk_0z}e^{j\omega t}. \quad (2)$$

The former part represents the RHCP component of the radiated field from the horn with a magnitude of F_{RH} while the second part is the LHCP component with a magnitude of F_{LH}.

Denoting the physical counterclockwise rotation angle of the mnth element by ψ_{mn}, the reflected RHCP field by the mnth S-shaped element can be written in the form

$$\vec{E}^{\text{refl}}_{\text{RHCP}} = |\Gamma_{\text{co-pol}}|\cdot F_{\text{RH}}\big(\overrightarrow{E_x} + j\overrightarrow{E_y}\big)e^{-jk_0z}e^{j\omega t}\cdot e^{-2j\psi_{mn}} + |\Gamma_{\text{cross-pol}}|\cdot F_{\text{LH}}\big(\overrightarrow{E_x} + j\overrightarrow{E_y}\big)e^{-jk_0z}e^{j\omega t}. \quad (3)$$

The first part represents the reflected RHCP field from the incident RHCP component of the feed horn, and thus a counterclockwise rotation angle ψ_{mn} of the element brings a $-2\psi_{mn}$ phase variation to the reflected co-pol field. The second part denotes the reflected RHCP field from the incident LHCP component of the feed horn, and no additional phase variation is introduced upon reflection [10].

Similarly, the reflected LHCP field by the mnth S-shaped element with rotation angle of ψ_{mn} can be represented by

$$\vec{E}^{\text{refl}}_{\text{LHCP}} = |\Gamma_{\text{co-pol}}|\cdot F_{\text{LH}}\big(\overrightarrow{E_x} - j\overrightarrow{E_y}\big)e^{-jk_0z}e^{j\omega t}\cdot e^{2j\psi_{mn}} + |\Gamma_{\text{cross-pol}}|\cdot F_{\text{RH}}\big(\overrightarrow{E_x} - j\overrightarrow{E_y}\big)e^{-jk_0z}e^{j\omega t}. \quad (4)$$

It is worth pointing out that $|\Gamma_{\text{cross-pol}}|$ used in (3) and (4) is of the same value due to reciprocity and thus is denoted by the same expression. Although the magnitudes of the reflection coefficient $|\Gamma_{\text{co-pol}}|$ are the same in (3) and (4), the phases of the reflection coefficient $\angle\Gamma_{\text{co-pol}}$ in these two cases differ in signs, i.e., $\angle\Gamma_{\text{co-pol}} = -2\psi_{mn}$ for a RHCP incident wave while $\angle\Gamma_{\text{co-pol}} = 2\psi_{mn}$ for a LHCP incident wave when the element is counterclockwise rotated by an angle of ψ_{mn} [10].

From (1), the condition for the aperture distribution to be cophasal in the desired direction $\overrightarrow{u_0}$ is

$$\phi_{mn} - k_0\big(\big|\overrightarrow{r_{mn}} - \overrightarrow{r_f}\big| + \overrightarrow{r_{mn}}\cdot\overrightarrow{u_0}\big) = 2k\pi, \quad k = 0, 1, 2\ldots \quad (5)$$

Here, the reflectarray is designed to radiate RHCP wave as its co-pol component. Thus, the co-pol component phase delay of the mnth element satisfies

$$-2\psi_{mn} - k_0\big(\big|\overrightarrow{r_{mn}} - \overrightarrow{r_f}\big| + \overrightarrow{r_{mn}}\cdot\overrightarrow{u_0}\big) = 2k\pi, \quad k = 0, 1, 2\ldots \quad (6)$$

Subsisting (3) and (6) into (1), the reradiated RHCP field of the reflectarray in the desired direction $\overrightarrow{u_0}$ can be represented by

$$E_{\text{RHCP}}\big(\overrightarrow{u_0}\big) = \sum_{m=1}^{15}\sum_{n=1}^{15} A\big(\overrightarrow{r_{mn}}\cdot\overrightarrow{u_0}\big) \times\Big\{|\Gamma_{\text{co-pol}}|\cdot F_{\text{RHCP}}\big(\overrightarrow{r_{mn}}\cdot\overrightarrow{r_f}\big)\cdot e^{j2k\pi} + |\Gamma_{\text{cross-pol}}| \cdot F_{\text{LHCP}}\big(\overrightarrow{r_{mn}}\cdot\overrightarrow{r_f}\big)\cdot e^{j2k\pi}e^{j2\psi_{mn}}\Big\} \quad (7)$$

where F_{RHCP} and F_{LHCP} denote the pattern function of the feed horn in RHCP and LHCP, respectively. Similarly, the reradiated LHCP field in the desired direction $\overrightarrow{u_0}$ can be written as

$$E_{\text{LHCP}}\big(\overrightarrow{u_0}\big) = \sum_{m=1}^{15}\sum_{n=1}^{15} A(\overrightarrow{r_{mn}}\cdot\overrightarrow{u_0}) \times\Big\{|\Gamma_{\text{co-pol}}|\cdot F_{\text{LHCP}}\big(\overrightarrow{r_{mn}}\cdot\overrightarrow{r_f}\big)\cdot e^{j2k\pi}e^{j4\psi_{mn}} + |\Gamma_{\text{cross-pol}}|F_{\text{RHCP}}\big(\overrightarrow{r_{mn}}\cdot\overrightarrow{r_f}\big)e^{j2k\pi}e^{j2\psi_{mn}}\Big\}. \quad (8)$$

For most of the elements, $\psi_{mn} \neq n\pi$, and it is evident that

$$\left|\sum_{m=1}^{15}\sum_{n=1}^{15} e^{j2\psi_{mn}}e^{j2k\pi}\right| < \left|\sum_{m=1}^{15}\sum_{n=1}^{15} e^{j2k\pi}\right| \qquad \left|\sum_{m=1}^{15}\sum_{n=1}^{15} e^{j4\psi_{mn}}e^{j2k\pi}\right| < \left|\sum_{m=1}^{15}\sum_{n=1}^{15} e^{j2k\pi}\right|. \quad (9)$$

Since $|F_{\text{RHCP}}(\overrightarrow{r_{mn}}\cdot\overrightarrow{r_f})| > |F_{\text{LHCP}}(\overrightarrow{r_{mn}}\cdot\overrightarrow{r_f})|$ in the main beam region when the feed horn is RHCP and $|\Gamma_{\text{co-pol}}| > |\Gamma_{\text{cross-pol}}|$ across the element's BW, it can be concluded from (7)–(9) that as follows.

1) To design an element rotated RHCP reflectarray with good performance in terms of antenna gain, the CP purity of the feed should be high. Otherwise, the incident LHCP field from the feed horn is dissipated according to (7) and (8), which wastes the incident LHCP power and results in a low gain and poor AE. Moreover, the reflected cross-pol component of the element should be low enough to keep the reflection of the incident RHCP field superposed in-phase. Otherwise, one part of the unwanted reflected field $|\Gamma_{\text{cross-pol}}|F_{\text{RHCP}}(\overrightarrow{r_{mn}}\cdot\overrightarrow{r_f})e^{j2k\pi}e^{j2\psi_{mn}}$ consumes the incident RHCP power substantially and also results in a decreased gain.
2) It is possible to get an enhanced AR from the reflectarray even with a feed which has a large AR. Particularly considering an LP feed, the incident RHCP and LHCP power upon the aperture is the same. From (7), the reflected RHCP field can be greatly improved if $|\Gamma_{\text{co-pol}}|$ is close to 1. Under the same condition, the reflected LHCP field is not superposed in-phase and thus is much smaller than the reflected RHCP field according to (8). Subsequently, the AR of the reflectarray is improved compared with the feed. However, the gain and AE of the reflectarray is reduced in this case since the incident LHCP power contributes little to the total gain as analyzed in conclusion (1).

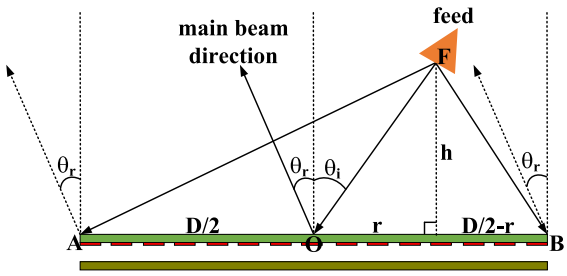

Fig. 10. Geometry of the reflectarray with arbitrary feed position and arbitrary main beam direction.

To verify the above analysis, the proposed reflectarray is illuminated by two different feed horns, one is a wideband dual-CP horn with RHCP port excited and another one is an ideal RHCP horn which has infinite CP BW and close to 0-dB AR. Besides, the aperture sizes of these two horns are all kept 50 mm × 50 mm to give a similar gain and beamwidth at each frequency. When conducting the comparison, the two different feeds are placed at the same position to make the f/D unchanged. With these conditions, the spillover under these two cases is considered to be close to each other.

Fig. 8 shows the simulated AR of the proposed reflectarray with different feed horns. As shown in Fig. 8, the AR BW (AR < 3 dB) of the dual-CP horn is from 6.7 to 11.5 GHz and the AR BW of the reflectarray using the dual-CP horn is from 7.2 to 14.7 GHz. From 6.7 to 7.2 GHz, the AR gets degraded from the horn to the array since the element reflection performance is rather bad in this frequency range. However, from 11.5 to 14.7 GHz, the AR of the array gets improved although the dual-CP horn demonstrates poor CP purity in this frequency range. This mainly attributes to the function of the array as indicated in the above conclusion (2).

Fig. 9 shows the simulated gain of the proposed reflectarray with different feed horns. As shown in Fig. 9, the gain of the reflectarray with dual-CP horn is smaller than the array with ideal horn from 11.5 to 15 GHz. As analyzed in the aforementioned conclusion (1), the poor CP purity of the dual-CP horn in this frequency range results in the nonnegligible LHCP incident field which contributes little to the gain of the array and yields a lower gain compared with the array using an ideal CP horn.

C. Effect of Differential Spatial Phase Delay

As indicated in Section III-B, the proposed reflectarray achieves a 2:1 3-dB AR BW. Due to this broad BW, it is necessary to investigate the influence of the differential spatial phase delay to the gain BW of the array, which increases as the working BW increases. The BW limitation of reflectarrays caused by the differential spatial phase delay is quantified for a broadside main beam and a prime focus feed in [25]. Here, equations are derived for more general cases, i.e., arbitrary feed position and arbitrary main beam direction to quantify the BW limitation of reflectarrays due to the differential spatial phase delay.

Fig. 10 shows the geometry of a reflectarray with arbitrary feed position and arbitrary main beam direction. As shown in Fig. 10, the diameter of the reflectarray is denoted by D while the focal length $f = \sqrt{r^2 + h^2}$. The feed horn is placed at an arbitrary position with an incident angle θ_i to the aperture center O and the main beam direction is denoted by θ_r.

Denoting the spatial phase delay from the feed to the aperture center O by $\mathrm{PD_{FO}}$ and the spatial phase delay from the feed to the edge of the aperture by $\mathrm{PD_{FA}}$ and $\mathrm{PD_{FB}}$. As the main beam direction is θ_r, the additional spatial phase delay introduced by the offset beam between the aperture center and the edge of the aperture is $(k_0 D \cdot \sin\theta_r)/2$. Therefore, the phase delay required by the aperture edge element A and B with respect to the aperture center O can be represented by $\mathrm{PD_{AO}}$ and $\mathrm{PD_{BO}}$, which satisfy

$$\begin{aligned} \mathrm{PD_{AO}} &= \mathrm{PD_{FA}} - \mathrm{PD_{FO}} - (k_0 D \cdot \sin\theta_r)/2 \\ \mathrm{PD_{BO}} &= \mathrm{PD_{FB}} - \mathrm{PD_{FO}} + (k_0 D \cdot \sin\theta_r)/2. \end{aligned} \tag{10}$$

Let k_1 and k_2 be the wavenumbers at the design frequency f_1 and operating frequency f_2, respectively. When the frequency shifts from the design frequency f_1 to the operating frequency f_2, phase errors will be introduced to each element. Denote the phase error at the edge element A and B, relative to the phase at the center element, by $\mathrm{PE_{AO}}$ and $\mathrm{PE_{BO}}$, which are

$$\begin{aligned} \mathrm{PE_{AO}} &= (k_2 - k_1) R_A \\ \mathrm{PE_{BO}} &= (k_2 - k_1) R_B \end{aligned} \tag{11}$$

where $R_A = (\sqrt{(D/2 + r)^2 + h^2} - \sqrt{r^2 + h^2} - (D \cdot \sin\theta_r)/2)$ and $R_B = (\sqrt{(D/2 - r)^2 + h^2} - \sqrt{r^2 + h^2} + (D \cdot \sin\theta_r)/2)$, calculating from the geometry relationship shown in Fig. 10. According to [25], a reasonable criterion for evaluating the effect of this phase error is to evaluate the frequency shift for which this error equals 180° at the edge of the aperture. The intervening elements will incur less phase error, but out-of-phase radiation from edge elements A and B will begin to detract from the overall gain of the aperture. Let $\mathrm{PE_{AO}}$ and $\mathrm{PE_{BO}}$ equal to 180° and solve the frequency shift, $\Delta f = f_2 - f_1$, we can get

$$\begin{aligned} \frac{\Delta f}{f_1} &= \frac{\lambda_1}{2R_A}, \quad \text{for } \mathrm{PE_{AO}} = \pi \\ \frac{\Delta f}{f_1} &= \frac{\lambda_1}{2R_B}, \quad \text{for } \mathrm{PE_{BO}} = \pi. \end{aligned} \tag{12}$$

Substituting geometry dimensions D, r, h, and θ_r given in Fig. 6(a) to (12), the frequency BW $2\Delta f/f_1$ for a circular aperture is roughly calculated to be 200% and 145.5%, respectively, for $\mathrm{PE_{AO}} = \pi$ and $\mathrm{PE_{BO}} = \pi$ (the design frequency f_1 is 9 GHz). As this calculated BW is wider than the element BW, the BW of the proposed reflectarray with 15 × 15 elements is mainly determined by the BW of elements and feed horn. But when the aperture size increases, the gain BW will decrease. Specifically, it can be calculated from (12) that the aperture diameter D equals to 540 and 396 mm, respectively for $\mathrm{PE_{AO}} = \pi$ and $\mathrm{PE_{BO}} = \pi$ if the BW $2\Delta f/f_1$ is set to be 66% (the element BW) and the f/D is kept unchanged. This indicates that the gain BW of the proposed reflectarray will begin to decrease if the aperture diameter exceeds 396 mm (roughly equivalent to a 280 mm × 280 mm square array).

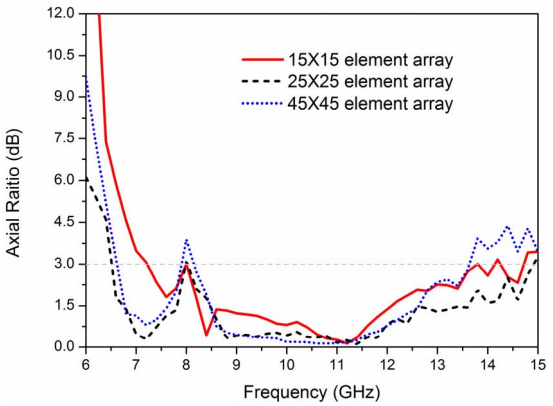

Fig. 11. Simulated AR of the reflectarray with elements of 15×15, 25×25, and 45×45.

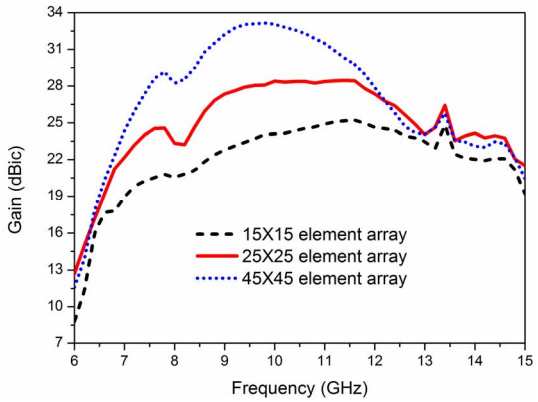

Fig. 12. Simulated gain of the reflectarray with elements of 15×15, 25×25, and 45×45.

D. Performance of S-Element-Based Reflectarrays With Larger Aperture Size

To analyze the performance of S-element-based reflectarrays with larger aperture size, another two arrays with elements of 25×25 (300 mm $\times$ 300 mm) and 45×45 (540 mm $\times$ 540 mm) are designed and simulated under the same f/D ratio as the 15×15 element array presented above. Fig. 11 shows the simulated AR of the reflectarray with different aperture sizes. As shown in Fig. 11, a 2:1 3-dB AR BW can be maintained when the aperture size increases. Compared with the 15×15 element array, the 3-dB AR BW of the 25×25 element array gets improved due to the fact that more elements are utilized, which makes the difference between the total reflected RHCP component and LHCP component larger than the case of 15×15 element array. When the array size increases to 540 mm $\times$ 540 mm, the AR performance gets improved before 13 GHz and degrades after 13 GHz since the phase error caused by the spatial phase delay at the frequencies higher than 13 GHz is rather large (design frequency is 9 GHz), which degrades the reflected RHCP component as well as the total antenna gain.

Fig. 12 shows the comparison of the simulated gain among the array with elements of 15×15, 25×25, and 45×45. As shown in Fig. 12, the 3-dB gain BW of the 15×15, 25×25, and 45×45 element array is 44.5%, 38.8%, and 30.6%, respectively. Although the 3-dB gain BW decreases as the aperture size increases, the proposed reflectarray with a large aperture size of 540 mm $\times$ 540 mm ($19.2\lambda \times 19.2\lambda$) still demonstrates much wider BW than other reported CP reflectarrays with large aperture size [10], [11] in terms of both 3-dB AR BW and 3-dB gain BW.

IV. Results and Discussion

A. Prototype and Reflection Coefficient

The fabricated prototype of the proposed antenna and the measurement setup in the anechoic chamber are shown in Fig. 13. As shown in Fig. 13, the reflectarray is fed by a wideband dual-CP horn which uses a stepped-septum polarizer to simultaneously achieve TE_{10} and TE_{01} modes as well as a 90° phase shift between the two orthogonal electric field components [26].

The simulated and measured reflection coefficients of the proposed reflectarray are shown in Fig. 14. As shown in Fig. 14, the array achieves a smaller than -10 dB reflection coefficient over a 2:1 frequency range. It is worthy pointing out that the S_{11} will degrade when a prime focus feed is utilized due to the blockage of the feed horn. To eliminate this phenomenon, an offset feed is chosen.

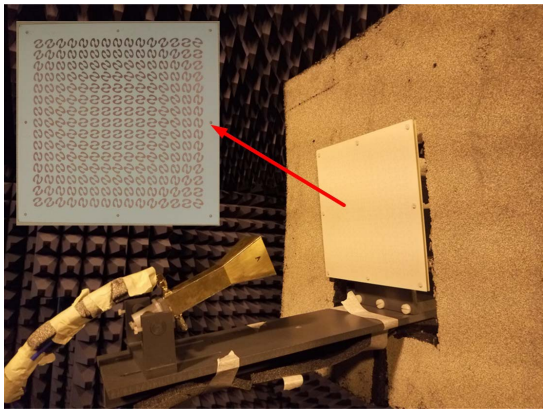

Fig. 13. Fabricated prototype and the measurement setup of the proposed antenna.

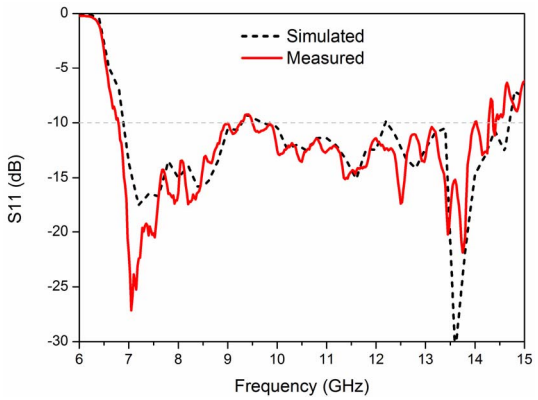

Fig. 14. Simulated and measured reflection coefficients of the reflectarray.

B. Axial Ratio

The simulated and measured AR of the proposed antenna are shown in Fig. 15. As shown in Fig. 15, the measured 3-dB

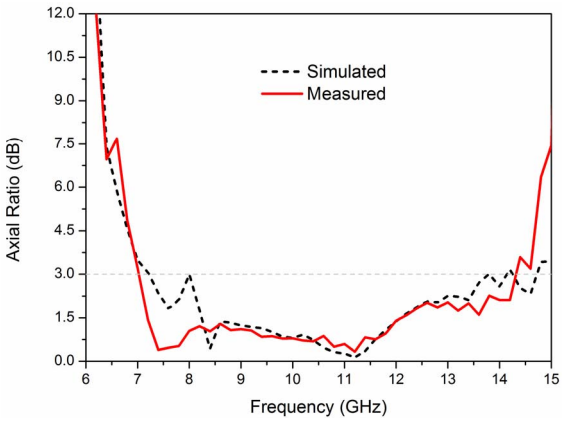

Fig. 15. Simulated and measured AR of the proposed antenna.

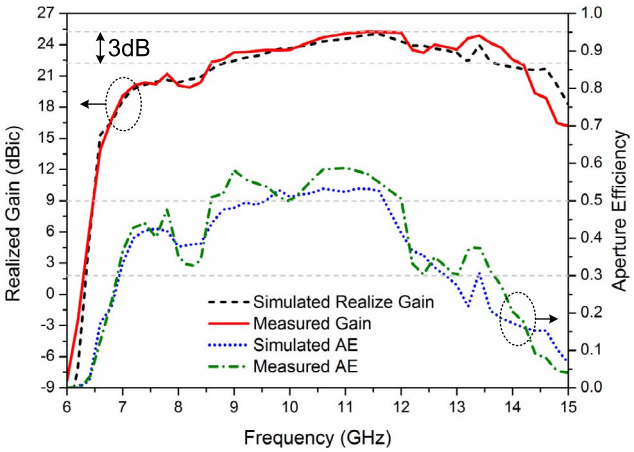

Fig. 16. Simulated and measured gain and efficiency of the proposed antenna.

AR BW is from 7 to 14.3 GHz, corresponding to a fractional BW of 68.5%.

C. Realized Gain and Aperture Efficiency

Fig. 16 shows the simulated realized gain and measured gain of the proposed reflectarray. It is shown that the realized gain decreases rapidly when the frequency is lower than 7 GHz. This is mainly caused by the drastic deterioration of the horn's reflection coefficient when the frequency exceeds the working frequency range of the horn, as shown in Fig. 14. As shown in Fig. 16, the measured 3-dB gain variation BW is from 8.6 to 14 GHz (47.8%). The measured gain peaks at 11.4 GHz with a value of 25.25 dBic.

The AE is also given by Fig. 16. The simulated AE is calculated based on the simulated realized gain while the measured AE is calculated by the measured gain. The difference between the results may stem from the fabrication errors of the horn and the array as well as the measurement errors. From the measured result, the reflectarray can achieve larger than 50% AE from 8.6 to 12 GHz (33%) and larger than 30% AE from 7 to 13.6 GHz (64%).

D. Radiation Pattern

As aforementioned, the proposed reflectarray achieves a nearly 2:1 BW in terms of impedance BW, 3-dB AR BW and 30% AE BW. Moreover, the proposed reflectarray can also maintain good radiation pattern performance such as undistorted radiation pattern shape, low sidelobe and low cross-pol component in a 2:1 BW. To verify this, the radiation patterns at five different frequencies are shown in Fig. 17. The main plane 1 in Fig. 17 refers to the xoz plane as shown in Fig. 6 while the main plane 2 is the plane perpendicular to main plane 1 along the main beam direction.

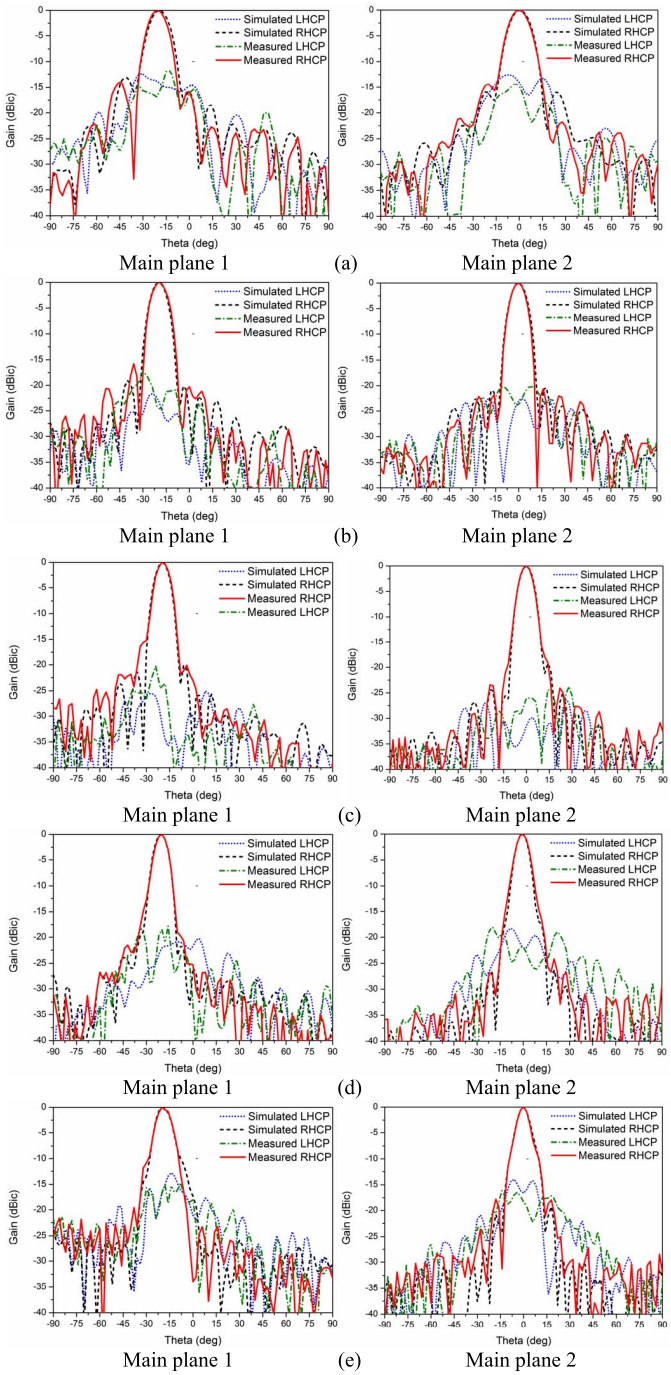

Fig. 17. Simulated and measured radiation patterns of the proposed antenna: (a) 7, (b) 9, (c) 10.6, (d) 12, and (e) 14 GHz.

As shown in Fig. 17, the measured radiation pattern agrees well with the simulated radiation pattern at each frequency. It is also observed from the results that the array maintains undistorted pencil-shaped beams, at least −15 dB sidelobe and −15 dB cross-pol component from 7 to 14 GHz.

TABLE II
COMPARISON WITH OTHER WIDEBAND CP REFLECTARRAYS

Ref. No.	Layers	Aperture Size (at center freq.)	f/D Ratio	Polarization of Feed	3-dB AR BW	Gain BW	AE BW	Peak Gain	Peak AE	Radiation Pattern BW
[9]	Single	6.7λ×6.7λ	0.84	LP	50%	1-dB gain 12.5%	-	24.4 dBic @12.5 GHz	46.3%	-
[17]	Single	9λ×9λ	1	LP	11%	1-dB gain 17%	-	25.8 dBic @9.8 GHz	39%	-
[18]	Dual	4.2λ×4.2λ	1	LP	28%	1-dB gain 20%	-	19.4 dBic @9.5 GHz	44%	-
[19]	Single	6.5λ×6.5λ	1	CP	43%	1-dB gain 31% 3-dB gain ~40%	-	~25 dBic @11.5 GHz	58.5%	-
[20]	Multi	Diameter:7.8λ	0.87	LP	40%	3-dB gain 40%	-	~25 dBic @11.5 GHz	~40%	40%
This work	Single	6.4λ×6.4λ	0.97	CP	68.5%	3-dB gain 47.8%	>50%: 33% >30%: 64%	25.2 dBic @11.6 GHz	60%	66.7%

E. Comparison With Other Wideband CP Reflectarrays

Due to the wideband characteristic of the novel S-shaped phasing element, the presented reflectarray achieves wide BW in all aspects. To demonstrate its advantages more clearly, a comparison between the proposed design and other reported wideband CP reflectarrays is given by Table II. As shown in Table II, the aperture size of the proposed design is comparable to the reference design [9], [19], [20] while it provides wider BW in terms of 3-dB AR BW, 3-dB gain BW, and radiation pattern BW. It is also noticed that the peak AE of the proposed reflectarray and [19] are much higher than the other designs with LP feed, which mainly attributes to the different element reflection performances under LP and CP incident waves. Moreover, the proposed reflectarray can maintain higher than 50% AE in a 33% BW and larger than 30% AE in a 64% BW, which also demonstrates its advantages over other designs.

V. CONCLUSION

A single-layer wideband CP reflectarray using a novel S-shaped phasing element is presented. The proposed S-shaped element achieves low cross-pol reflection and very linear phase shift to the element rotation angle in a 2:1 BW. Theoretical analysis indicates that the AR BW of the CP reflectarray can be improved using element rotation method even with incident fields poor in CP purity. Moreover, the differential spatial phase delay is proven to have little effect to the BW of small sized array but degrades the BW of large sized array. The measurement results demonstrate that the proposed reflectarray has a 68.5% 3-dB AR BW and a 47.8% 3-dB gain BW. More importantly, the AE of the proposed array is larger than 50% in a 33% BW and larger than 30% in a 64% BW. These excellent performances make the proposed reflectarray a good candidate for high-data-rate satellite communications.

REFERENCES

[1] J. Huang and J. A. Encinar, *Reflectarray Antennas*. Hoboken, NJ, USA: Wiley, 2007.
[2] J. A. Encinar and J. A. Zornoza, "Broadband design of three-layer printed reflectarrays," *IEEE Trans. Antennas Propag.*, vol. 51, no. 7, pp. 1662–1664, Jul. 2003.
[3] J. A. Encinar, "Design of two-layer printed reflectarrays using patches of variable size," *IEEE Trans. Antennas Propag.*, vol. 49, no. 10, pp. 1403–1410, Oct. 2001.
[4] P.-Y. Qin, Y. J. Guo, and A. R. Weily, "Broadband reflectarray antenna using subwavelength elements based on double square meander-line rings," *IEEE Trans. Antennas Propag.*, vol. 64, no. 1, pp. 378–383, Jan. 2016.
[5] Y. Mao, S. Xu, F. Yang, and A. Z. Elsherbeni, "A novel phase synthesis approach for wideband reflectarray design," *IEEE Trans. Antennas Propag.*, vol. 63, no. 9, pp. 4189–4193, Sep. 2015.
[6] E. Carrasco, J. A. Encinar, and M. Barba, "Bandwidth improvement in large reflectarrays by using true-time delay," *IEEE Trans. Antennas Propag.*, vol. 56, no. 8, pp. 2496–2503, Aug. 2008.
[7] S. Gao, Q. Luo, and F. Zhu, *Circularly Polarized Antennas*. Hoboken, NJ, USA: Wiley, 2013.
[8] Y. Li, M. E. Bialkowski, and A. M. Abbosh, "Single layer reflectarray with circular rings and open-circuited stubs for wideband operation," *IEEE Trans. Antennas Propag.*, vol. 60, no. 9, pp. 4183–4189, Sep. 2012.
[9] G.-B. Wu, S.-W. Qu, S. Yang, and C. H. Chan, "Broadband, single-layer dual circularly polarized reflectarrays with linearly polarized feed," *IEEE Trans. Antennas Propag.*, vol. 64, no. 10, pp. 4235–4241, Oct. 2016.
[10] J. Huang and R. J. Pogorzelski, "A Ka-band microstrip reflectarray with elements having variable rotation angles," *IEEE Trans. Antennas Propag.*, vol. 46, no. 5, pp. 650–656, May 1998.
[11] A. Yu, F. Yang, A. Z. Elsherbeni, J. Huang, and Y. Kim, "An offset-fed X-band reflectarray antenna using a modified element rotation technique," *IEEE Trans. Antennas Propag.*, vol. 60, no. 3, pp. 1619–1624, Mar. 2012.
[12] R. Deng, Y. Mao, S. Xu, and F. Yang, "A single-layer dual-band circularly polarized reflectarray with high aperture efficiency," *IEEE Trans. Antennas Propag.*, vol. 63, no. 7, pp. 3317–3320, Jul. 2015.
[13] R. S. Malfajani and Z. Atlasbaf, "Design and implementation of a dual-band single layer reflectarray in X and K bands," *IEEE Trans. Antennas Propag.*, vol. 62, no. 8, pp. 4425–4431, Aug. 2014.
[14] C. Han, J. Huang, and K. Chang, "A high efficiency offset-fed X/ka-dual-band reflectarray using thin membranes," *IEEE Trans. Antennas Propag.*, vol. 53, no. 9, pp. 2792–2798, Sep. 2005.
[15] T. Smith, U. Gothelf, O. S. Kim, and O. Breinbjerg, "An FSS-backed 20/30 GHz circularly polarized reflectarray for a shared aperture L- and Ka-band satellite communication antenna," *IEEE Trans. Antennas Propag.*, vol. 62, no. 2, pp. 661–668, Feb. 2014.
[16] W. A. Imbriale, S. Gao, and L. Boccia, *Space Antenna Handbook*. Hoboken, NJ, USA: Wiley, 2012.
[17] G. Zhao, Y.-C. Jiao, F. Zhang, and F.-S. Zhang, "A subwavelength element for broadband circularly polarized reflectarrays," *IEEE Antennas Wireless Propag. Lett.*, vol. 9, pp. 330–333, 2010.
[18] L.-S. Ren, Y.-C. Jiao, F. Li, J.-J. Zhao, and G. Zhao, "A dual-layer T-shaped element for broadband circularly polarized reflectarray with linearly polarized feed," *IEEE Antennas Wireless Propag. Lett.*, vol. 10, pp. 407–410, 2011.
[19] M.-Y. Zhao, G.-Q. Zhang, X. Lei, J.-M. Wu, and J.-Y. Shang, "Design of new single-layer multiple-resonance broadband circularly polarized reflectarrays," *IEEE Antennas Wireless Propag. Lett.*, vol. 12, pp. 356–359, 2013.

[20] S. M. A. M. H. Abadi and N. Behdad, "Broadband true-time-delay circularly polarized reflectarray with linearly polarized feed," *IEEE Trans. Antennas Propag.*, vol. 64, no. 11, pp. 4891–4896, Nov. 2016.
[21] L. Zhang, S. Gao, Q. Luo, P. R. Young, W. Li, and Q. Li, "Inverted-S antenna with wideband circular polarization and wide axial ratio beamwidth," *IEEE Trans. Antennas Propag.*, vol. 65, no. 4, pp. 1740–1748, Apr. 2017.
[22] A. Mahmoud, A. A. Kishk, Z. Hao, and W. Hong, "Ka-band circularly polarized reflectarray: Using a double-layers cross slot," *IEEE Antennas Propag. Mag.*, vol. 58, no. 4, pp. 60–68, Aug. 2016.
[23] D. M. Pozar, S. D. Targonski, and H. D. Syrigos, "Design of millimeter wave microstrip reflectarrays," *IEEE Trans. Antennas Propag.*, vol. 45, no. 2, pp. 287–296, Feb. 1997.
[24] P. Nayeri, A. Z. Elsherbeni, and F. Yang, "Radiation Analysis Approaches for Reflectarray Antennas," *IEEE Antennas Propag. Mag.*, vol. 55, pp. 127–134, 2013.
[25] D. M. Pozar, "Bandwidth of reflectarrays," *Electron. Lett.*, vol. 39, no. 21, pp. 1490–1491, Oct. 2003.
[26] J. Bornemann and V. A. Labay, "Ridge waveguide polarizer with finite and stepped-thickness septum," *IEEE Trans. Microw. Theory Techn.*, vol. 43, no. 8, pp. 1782–1787, Aug. 1995.

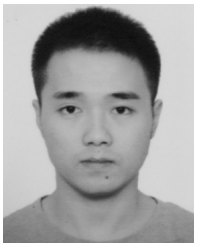

Long Zhang received the B.S. and M.S. degrees in electrical engineering from the Huazhong University of Science and Technology, Wuhan, China, in 2009 and 2012, respectively, and the Ph.D. degree in electronic engineering from the University of Kent, Canterbury, U.K, in 2017.

He is currently an Assistant Professor with the College of Information Engineering, Shenzhen University, Shenzhen, China. His current research interests include circularly polarized antennas, smart antennas, reconfigurable antennas, mobile terminal antennas, phased arrays, tightly coupled arrays, and reflectarrays.

Steven Gao (M'01–SM'16) received the Ph.D. degree in microwave engineering from Shanghai University, Shanghai, China, in 1999.

He is a Professor and the Chair in RF and microwave engineering with the University of Kent, Canterbury, U.K. He has co-authored two books including *Space Antenna Handbook* (Wiley, 2012) and *Circularly Polarized Antennas* (IEEE-Wiley, 2014), authored more than 250 papers, and holds several patents in smart antennas and RF. His current research interests include smart antennas, phased arrays, satellite antennas, RF/microwave/mm-wave/THz circuits, satellite communications, ultra-wideband (UWB) radars, synthetic-aperture radars, and mobile communications.

Qi Luo (S'08–M'12) received the M.Sc degree in data communications from the University of Sheffield, Sheffield, U.K., in 2006, and the Ph.D. degree in electrical engineering from the University of Porto, Porto, Portugal, in 2012.

From 2012 to 2013, he was a Research Fellow with the Surrey Space Center, Guildford, U.K. He is currently a Research Associate with the School of Engineering and Digital Arts, University of Kent, Canterbury, U.K. His current research interests include smart antennas, circularly polarized antennas, reflectarray, multiband microstrip antennas, and electrically small antenna design.

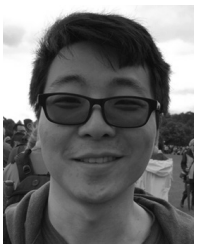

Wenting Li received the B.S. degree in electronic information engineering and the M.S. degree in electromagnetic field and microwave technology from Northwestern Polytechnical University, Xi'an, China, in 2011 and 2014, respectively. He is currently pursuing the Ph.D. degree with the University of Kent, Canterbury, U.K.

His current research interests include reflectarray antennas, reconfigurable antennas, circularly polarized antennas, and multibeam antennas.

Yejun He (SM'09) received the Ph.D. degree in information and communication engineering from Huazhong University of Science and Technology, Wuhan, China, in 2005.

From 2005 to 2006, he was a Research Associate with the Department of Electronic and Information Engineering, Hong Kong Polytechnic University, Hong Kong. From 2006 to 2007, he was a Research Associate with the Department of Electronic Engineering, Faculty of Engineering, Chinese University of Hong Kong, Hong Kong. In 2012, he was a Visiting Professor with the Department of Electrical and Computer Engineering, University of Waterloo, Waterloo, ON, Canada. From 2013 to 2015, he was an Advanced Visiting Scholar (Visiting Professor) with the School of Electrical and Computer Engineering, Georgia Institute of Technology, Atlanta, GA, USA. Since 2011, he has been a Full Professor with the College of Information Engineering, Shenzhen University, Shenzhen, China, where he is the Director of Guangdong Engineering Research Center of Base Station Antennas and Propagation, and the Director of Shenzhen Key Laboratory of Antennas and Propagation, Shenzhen. He has authored or co-authored more than 100 research papers, books (chapters) and holds 13 patents. His current research interests include channel coding and modulation, 4G/5G wireless mobile communication, space-time processing, antennas, and RF.

Dr. He is a Fellow of IET. He served as a Technical Program Committee Member or a Session Chair for various conferences, including the IEEE Global Telecommunications Conference (GLOBECOM), the IEEE International Conference on Communications, the IEEE Wireless Communication Networking Conference, and the IEEE Vehicular Technology Conference. He is an Associate Editor of the IEEE ACCESS and the *Security and Communication Networks*. He has served as a Reviewer for various journals such as the IEEE TRANSACTIONS ON VEHICULAR TECHNOLOGY, the IEEE TRANSACTIONS ON COMMUNICATIONS, the IEEE TRANSACTIONS ON WIRELESS COMMUNICATIONS, the IEEE TRANSACTIONS ON INDUSTRIAL ELECTRONICS, the *IEEE Wireless Communications*, the *IEEE Communications Letters, IEEE Journal on Selected Areas in Communications*, the *International Journal of Communication Systems*, the *Wireless Communications and Mobile Computing*, and the *Wireless Personal Communications*. He is the Principal Investigator for over 20 current or finished research projects including NSFC of China, the Integration Project of Production Teaching and Research by Guangdong Province and Ministry of Education as well as the Science and Technology Program of Shenzhen City.

Qingxia Li (M'08) received the B.S., M.S., and Ph.D. degrees in electrical engineering from Huazhong University of Science and Technology (HUST), Wuhan, China, in 1987, 1990, and 1999, respectively.

He is currently a Professor with the Science and Technology on Multispectral Information Processing Laboratory, School of Electronic Information and Communications, HUST. His current research interests include microwave remote sensing and deep space exploration, electromagnetic theory and application, antenna array, and signal processing.